European Conference on Computational Fluid Dynamics
ECCOMAS CFD 2006
P. Wesseling, E. Oñate and J. Périaux (Eds)

DESIGN EXPLORATION OF SHIELDING EFFECT FOR AIRCRAFT ENGINE NOISE

Kazuhisa Chiba*, **Taro Imamura***, **Kazuhisa Amemiya**†, **Shinkyu Jeong**‡, **and Kazuomi Yamamoto***

*Japan Aerospace Exploration Agency
7-44-1 Jindaiji-Higashi, Chofu, Tokyo 182-8522, Japan
e-mail: chiba@chofu.jaxa.jp
web page: http://www.jaxa.jp/index_e.html

†Foundation for Promotion of Japanese Aerospace Technology
1-16-6 Izumi-Chuo, Izumi, Sendai 981-3133, Japan
webpage: http://f-jaxt.or.jp/

‡Tohoku University
2-1-1 Katahira, Aoba, Sendai 980-8577, Japan
web page: http://www.ifs.tohoku.ac.jp/edge/indexe.html

Key words: Computational Aeroacoustics, Aircraft Engine Noise, Shielding Effect, Design Exploration, Data Mining, Self-Organizing Map

Abstract. *The multi-objective design exploration of the two-dimensional shielding effect for engine noise using V-tale wing has been performed. Two objective functions are considered as the minimization of the sound pressure level at the side and bottom locations relative to the fuselage, which values are evaluated by using the linearized Euler equation. Two design variables are defined as the wing length and the wing cant angle to set on the fuselage. The response surface method with kriging model is employed as the optimizer to reduce the time required for design exploration. As a result, there is no tradeoff between two objective functions, i.e., the sound pressure level at the side and bottom measuring locations can be reduced, simultaneously. The wing cant angle which is set at nearly 65 deg is most effective to shield the noise. It is justly the necessary condition to reduce the sound pressure level that the wing length becomes long. Moreover, a self-organizing map as a data mining technique obtains the knowledge in the design space regarding the correlation between the objective functions and the design variables.*

1 INTRODUCTION

The engine noise reduction is one of the most important for jet aircraft design. Although the devices for engine itself is investigated as the manner for the aircraft noise reduction, their improvement reaches the ceiling and other manners should be considered which huge reduction is anticipated. One of the considerable manner is the shielding effect using wing and fuselage[1] when a conventional geometry is considered. That is, as an engine is mounted above a aft-circular fuselage portion and V-tale wing is set on that fuselage, the huge noise reduction is fulfilled. In the present study, the two-dimensional problem is defined to confirm the shielding effect. The objective of the present study is the investigation of the two-dimensional shielding effect regarding the wing cant angle relative to the fuselage and wing length through multi-objective design exploration.

The prediction of the aerodynamic sound induced by the unsteady flow field is important. There are various approaches to simulate the flow field with sound propagation. The direct numerical simulation (DNS) which treat a density variation associated with a sound generation is a leading candidate for accurate simulation for the generation and propagation of aerodynamic sound. However, DNS is quite costly computation. The other hand, the computation based on the linearized Euler equation (LEE) is one of the accurate method capturing the propagation of sound. The essential key of this method is to reduce the computational time compared with DNS. That is, this method can be employed as an evaluation method for an optimization or a design exploration problem regarding noise reduction. The present study is the first trial for the design exploration of a silent aircraft design.

2 MULTI-OBJECTIVE DESIGN EXPLORATION

2.1 Objective Functions

Two objective functions are defined as the minimization of the sound pressure level (SPL) at the side and bottom locations relative to the fuselage, because these measuring locations are defined by International Civil Aviation Organization. The evaluation positions are set on (0, 2.5) and (-2.5, 0) shown in Fig. 1. The evaluation values in optimizer are considered as the integration value of sound pressure level for one wavelength.

2.2 Geometry Definition

It is assumed that an engine is mounted above an aft-fuselage portion, the shielding effect is investigated on the plane to cut the aft-fuselage in round slices. The cross section of the fuselage is defined by a circle. When its diameter is 3m, the mono-pole sound source is set over 0.45m from the top of fuselage shown in Fig. 1. That is, it is assumed that the sound source of engine noise is the mono-pole in this study. When the reference length is 3m, the frequency of mono-pole sound source is approximately 500Hz. Although the practical frequency of engine noise is higher, it takes impractical time to evaluate because necessary mesh resolution becomes fine. It takes roughly four hours for the mesh with the resolution for 500Hz using five CPUs of a PC cluster with Pentium IV 2.2GHz processors.

The wing is defined by the two design variables as the cant angle γ relative to the fuselage and the spanwise length ℓ. The thickness is ignored because the wing is defined by giving of the wall boundary condition on mesh block boundary. The constraints in an op-

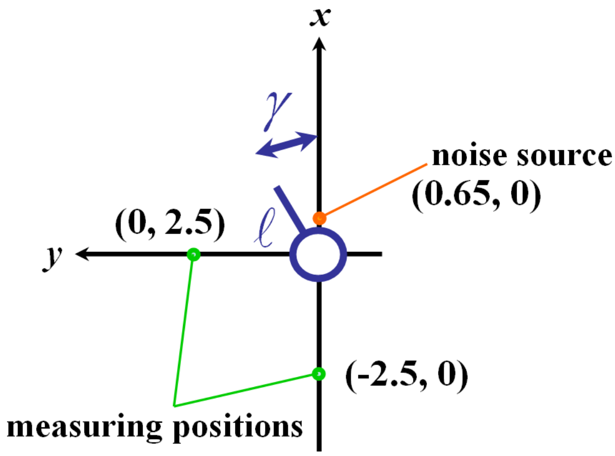

Figure 1: Defined coordinate. The values are normalized by the fuselage diameter as the reference length.

Table 1: Particularity of two design variables.

serial number	*correspondent design variable*	
1	wing cant angle γ	$30\text{deg} \leq \gamma \leq 120\text{deg}$
2	wing spanwise length ℓ	$1.2\text{m} \leq \ell \leq 5.7\text{m}$

timizer is considered for the wing geometry, *i.e.*, the design variables. The particularities of the constraints are summarized in Table 1.

2.3 Evaluation Method

For the evaluation method regarding the engine noise, the linearized-Euler equation coupled with unified platform for aerospace computational simulation (UPACS-LEE) as an in-house computational aeroacoustics (CAA) solver[2] is employed on the multi-block structured mesh generated for aeroacoustic analysis shown in Fig. 2.

The fluctuation $[\rho', (\rho u_i)', E']$ is computed using the given computational conditions of averaged physical variables $[\rho, \rho u_i, E]$ and sound sources $[S_\rho, S_{\rho u_i}, S_E]$ in LEE. In the present study, the mono-pole sound source is given by the following equation to focus the propagation analysis of LEE code.

$$\boldsymbol{S} = \begin{bmatrix} S_\rho \\ S_{\rho u_i} \\ S_E \end{bmatrix} = \begin{bmatrix} S \\ \overline{u_i} S \\ \left(\dfrac{c^2}{\gamma - 1} + \dfrac{1}{2} \overline{u_k}^2 \right) S \end{bmatrix} \tag{1a}$$

$$S = A \exp \left[-(\ln 2) \left(\frac{(x - x_s)^2 + (y - y_s)^2}{b^2} \right) \right] \sin \omega t \tag{1b}$$

where c denotes the speed of sound and S is the Gaussian distribution. (x, y) and t represent the coordinates and time, respectively. A, b, (x_s, y_s), and ω denote amplitude, the width of the Gaussian distribution at half value, the coordinates of the sound source, and the angular frequency of the mono-pole, respectively. The UPACS-LEE employs the sixth-order compact scheme suggested by Kobayashi[3], the 10th-order filter suggested by Gaitonde-Visbal[4] to restrain the computational vibration, and fourth-order Jameson-Baker Runge-Kutta method[5] for the time integration.

In the present study, the sponge region[6] is generated on far field to absorb sound wave. The boundary condition for slip wall suggested by Chakravarthy *et al.*[7] is used for the wall boundary condition.

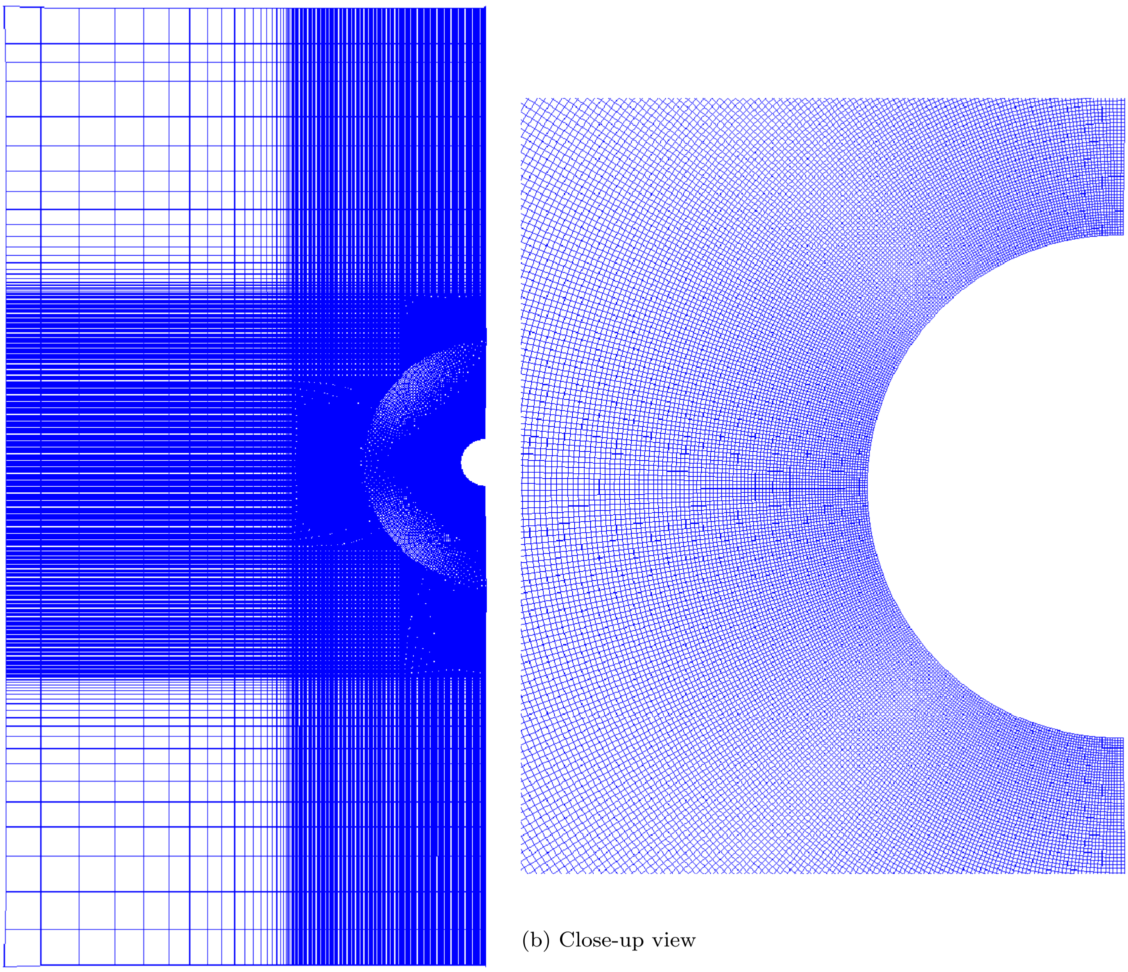

(b) Close-up view

(a) Overview

Figure 2: Generated mesh.

2.4 Optimizer

The most obvious forms of regression are those using least-squares polynomials. However, they are not good at modeling complex surfaces that have many local basins and bulges in them. In the present study, a kriging approach[8, 9] is used instead because this allows the use to control the amount of regression as well as providing a theoretically sound basis for judging the degree of curvature needed to model adequately the user's data. In addition, kriging provides measures of probable errors in model being built that can be used when assessing where to place any further design points.

In kriging, the inputs $\boldsymbol{x}$ are assumed to be related to the outputs, that is, responses y by an expensive function $f_e(\boldsymbol{x})$. Here, this function is UPACS-LEE code to analyze sound pressure. The response of the code is then evaluated for combinations of inputs generated by the the design of experiments (DOE) with D-optimality and used to construct an approximation.

The present kriging model describes the unknown function $y(\boldsymbol{x})$ as follows;

$$y(\boldsymbol{x}) = \beta + Z(\boldsymbol{x}) \tag{2}$$

where $\boldsymbol{x}$ is an m-dimensional vector (m design variables), β denotes a constant global model, and $Z(\boldsymbol{x})$ represents a local deviation from the global model. In kriging, Z is taken to depend on the distance between corresponding points. The distance measure is employed instead of the Euclidean distance as follows;

$$d\left(\boldsymbol{x}^{(i)}, \boldsymbol{x}^{(j)}\right) = \sum_{h=1}^{k} \theta_h \left| x_h^{(i)} - x_h^{(j)} \right|^2 \tag{3}$$

where θ_h denotes the k-th element of the correlation vector parameter $\boldsymbol{\theta}$. The correlation $\boldsymbol{R}$ between points $\boldsymbol{x}^{(i)}$ and $\boldsymbol{x}^{(j)}$ is given as follows;

$$\boldsymbol{R}\left(\boldsymbol{x}^{(i)}, \boldsymbol{x}^{(j)}\right) = \exp\left[-d\left(\boldsymbol{x}^{(i)}, \boldsymbol{x}^{(j)}\right)\right] \tag{4}$$

When the response at a new point $\boldsymbol{x}$ is required, a vector of correlations between the point and those used in the DOE is formed, $\boldsymbol{r}(\boldsymbol{x}) = \boldsymbol{R}(\boldsymbol{x}, \boldsymbol{x}^i)$. The prediction is then given by

$$\hat{y}(\boldsymbol{x}) = \hat{\beta} + \boldsymbol{r}^T \boldsymbol{R}^{-1} \left(\boldsymbol{y} - \boldsymbol{I}\hat{\beta}\right) \tag{5}$$

where $\hat{\beta}$ denotes the estimated value of β and $\boldsymbol{y} = [y(x)^1, \cdots, y(x)^n]$.

The unknown parameter to be estimated for constructing the kriging model is $\boldsymbol{\theta}$. This parameter can be estimated by maximizing the following likelihood function f_ℓ

$$f_\ell\left(\hat{\beta}, \hat{\sigma}^2, \boldsymbol{\theta}\right) = \frac{1}{(2\pi)^{n/2}(\hat{\sigma}^2)^{n/2}|\boldsymbol{R}|^{1/2}} \exp\left[\frac{-(\boldsymbol{y} - \boldsymbol{I}\hat{\beta})^T \boldsymbol{R}^{-1}(\boldsymbol{y} - \boldsymbol{I}\hat{\beta})}{2\hat{\sigma}^2}\right] \tag{6}$$

Maximizing the likelihood function is an m-dimensional unconstrained nonlinear optimization problem. In this study, the alternative method is employed to solve this problem. For a given $\boldsymbol{\theta}$, $\hat{\beta}$ and $\hat{\sigma}^2$ is defined as

$$\hat{\beta} = \frac{\boldsymbol{I}^T \boldsymbol{R}^{-1} \boldsymbol{y}}{\boldsymbol{I}^T \boldsymbol{R}^{-1} \boldsymbol{I}} \tag{7a}$$

$$\hat{\sigma}^2 = (\boldsymbol{y} - \boldsymbol{I}\hat{\beta})^T \boldsymbol{R}^{-1} (\boldsymbol{y} - \boldsymbol{I}\hat{\beta})/n \tag{7b}$$

n is the number of points used in the DOE. The mean-squared error of the prediction is

$$s^2(\boldsymbol{x}) = \hat{\sigma}^2 \left[1 - \boldsymbol{r}^T \boldsymbol{R}^{-1} \boldsymbol{r} + \frac{(1 - \boldsymbol{I}^T \boldsymbol{R}^{-1} \boldsymbol{r})^2}{\boldsymbol{I}^T \boldsymbol{R}^{-1} \boldsymbol{I}} \right] \tag{8}$$

The root mean squared error (RMSE) is described as $s = \sqrt{s^2(\boldsymbol{x})}$.

3 RESULTS OF DESIGN EXPLORATION

The design variable as the cant angle is chosen at every 10deg and the design variable as the length is chosen at every 0.9m. The 25 couples are extracted from a total number of 60 by using the DOE for the initial sample points of the kriging model. Three additional sample points are added per one update, which include two weak and one strong non-dominated solutions. And then, update is stopped when the optimum solutions are converged. No flow condition is assumed.

Exact and the approximate solutions obtained by a kriging-based response surfaces are shown in Fig. 3. This figure shows that both objective functions can be minimized simultaneously, *i.e.*, there is no severe tradeoff between the objective functions in the present design space. Pareto surface does not focus on a point, it has width. This shows that the evaluated values of the present objective functions include perturbation due to unsteady phenomenon.

The kriging-based response surfaces for the objective functions are shown in Fig. 4. The comparison of these two figures reveals that the location to reduce SPL is similar, and there is no tradeoff between the objective functions. Moreover, the cant angle to reduce SPL is from 65 to 68deg, which value is expedient for realistic development of V-tale wing. The reduction of the present objective functions depends on the cant angle. When the appropriate cant angle is designed, the SPL is reduced as long as the wing length can. Figure 4(a) shows the response surface at the side measuring location. This figure reveals that the SPL at the side location is always great, when the cant angle surpasses 90deg. Because there is no shield for the sound pressure from the noise source. It does not depend on the wing length for that situation.

Figure 5 shows the comparison of the root mean square (RMS) distribution of sound pressure fluctuation using log scale between no wing and V-tale one. When there is no wing, two strong pressure distributions occur near the noise source. One radiates to diagonally above the fuselage, the other occurs to sideward of the fuselage. The wing

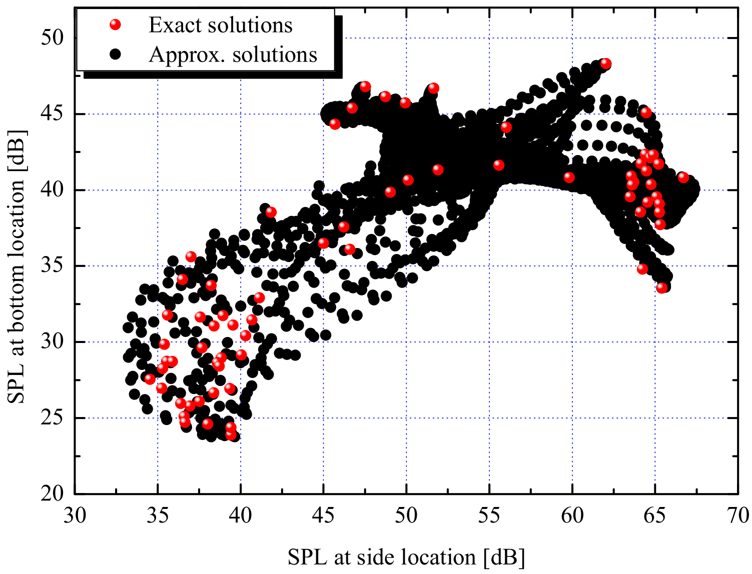

Figure 3: Exact and approximate solutions obtained by kriging-based response surface method plotted in the two-dimensional plane of the objective functions.

should properly shield this sideward radiation to reduce the SPL at the side location. The right side of Fig. 5 shows the RMS distribution of the sound pressure fluctuation with V-tale wing of the cant angle of 67deg and the length of 5.1m, which design variables give one of the strong non-dominated solutions. This wing effectively shields the strong sideward radiation, and the value at side and bottom locations is restrained, simultaneously. That is, it is essential key of the effective shielding to restrain the radiation to sideward of the fuselage.

4 DATA MINING

4.1 Self-Organizing Map

4.1.1 General SOM Algorithm

SOM[10] is an unsupervised learning, nonlinear projection algorithm from high to low-dimensional space. This projection is based on self-organization of a low-dimensional array of neurons. In the projection algorithm, the weights between the input vector and the array of neurons are adjusted to represent features of the high dimensional data on the low-dimensional map. The close two patterns are in the original space, the closer is the response of two neighboring neurons in the low-dimensional space. Thus, SOM reduces the dimension of input data while preserving their features.

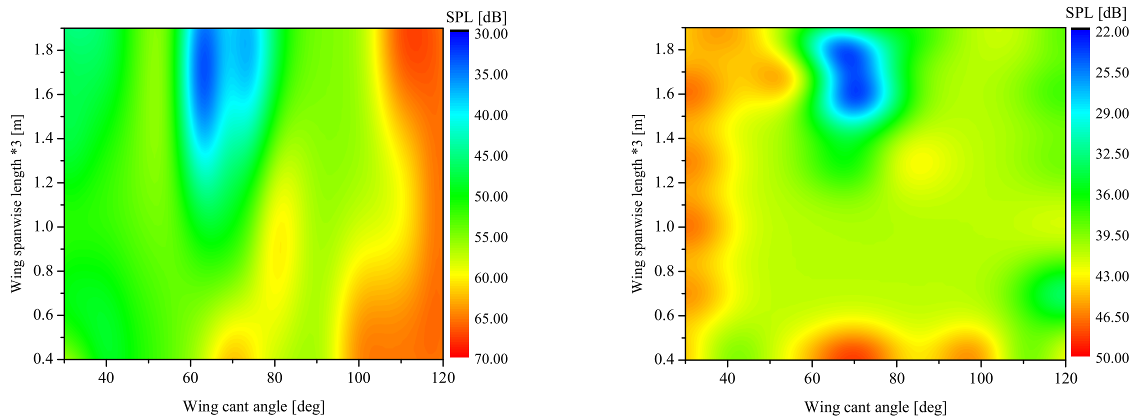

(a) Colored by the SPL at the side measuring location

(b) Colored by the SPL at the bottom measuring location

Figure 4: Response surface of the objective functions for the design variables.

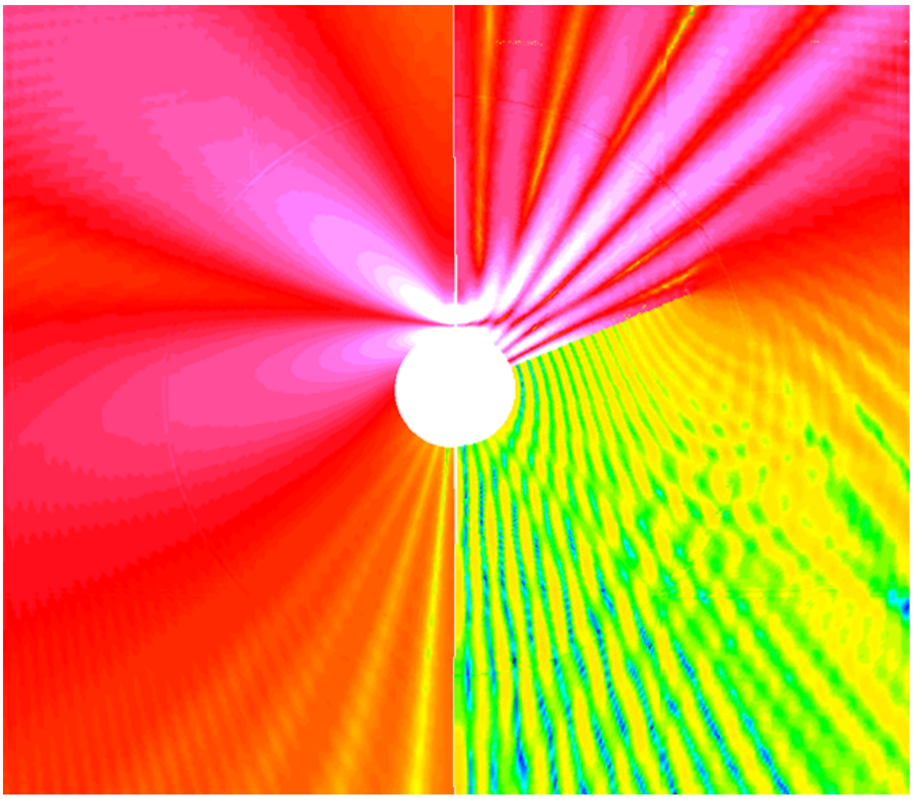

Figure 5: Comparison of the root mean square distribution of sound pressure fluctuation using log scale between no wing (left) and V-tale wing of the cant angle of 67deg and the length of 5.1m (right).

4.1.2 Batch-SOM

In this study, SOMs are generated by using commercial software Viscovery® SOMine plus 4.0[11] produced by Eudaptics GmbH. Although SOMine is based on the general SOM concept and algorithm, it employs an advanced variant of unsupervised neural networks, *i.e.*, Kohonen's Batch SOM[12, 13]. The algorithm consists of two steps that are iterated until no more significant changes occur: search of the best-matching unit c_i for all input data $\{\boldsymbol{x}_i\}$ and adjustment of weight vector $\{\boldsymbol{m}_j\}$ near the best-matching unit. The Batch-SOM algorithm can be formulated as follows:

$$c_i = \arg\min \|\boldsymbol{x}_i - \boldsymbol{m}_j\| \tag{9a}$$

$$\boldsymbol{m}_j^* = \frac{\displaystyle\sum_i h_{jc_i}\boldsymbol{x}_i}{\displaystyle\sum_i h_{jc_i}} \tag{9b}$$

where $\boldsymbol{m}_j^*$ is the adjusted weight vector. The neighborhood relationship between two neurons j and k is defined by the following Gaussian-like function:

$$h_{jk} = \exp\left(-\frac{d_{jk}^2}{r_t^2}\right) \tag{10}$$

where d_{jk} denotes the Euclidean distance between the neuron j and the neuron k on the map, and r_t is the neighborhood radius which is decreased with the iteration steps t.

The standard Kohonen algorithm adjusts the weight vector after all each record is read and matched. On the contrary, the Batch-SOM takes a 'batch' of data (typically all records), and performs a 'collected' adjustment of the weight vectors after all records have been matched. This is much like 'epoch' learning in supervised neural networks. The Batch-SOM is a more robust approach, since it mediated over a large number of learning steps. In the SOMine, the uniqueness of the map is ensured by the adoption of the Batch-SOM and the linear initialization for input data. Much like some other SOMs[14], SOMine creates a map in a two-dimensional hexagonal grid. Starting from numerical, multivariate data, the nodes on the grid gradually adapt to the intrinsic shape of the data distribution can be read off from the emerging map on the grid. The trained SOM is systematically converted into visual information[15, 16].

4.2 Design Knowledge

The SOMs are generated by using 70 exact solutions explored by the kriging model because the strict correlation between the objective functions and the design variables is investigated. Figure 6 shows the SOMs colored by the objective functions and the design variables. Figures 6(a) and (b) have low value on the lower right corner. It reveals that both of the objective functions can be reduced simultaneously, *i.e.*, there is no tradeoff between them, and the sweet spot exists in the present design space.

Figures 6(a) and (c) have high value on the upper region. It shows that the SPL at the side measuring location becomes high when the cant angle is higher than 90deg. This corresponds to the fact that the SPL becomes high because the strong sound pressure radiated to the sideward shown in Fig. 5 is not shielded.

When the left region on Fig. 6(c) is low, the same region on Fig. 6(b) has high. That is, when the cant angle becomes low, the SPL at the bottom measuring location is increased. This is the reason the SPL of whole locations becomes high due to the reflection and diffraction of the strong sound pressure around the wing. This phenomenon does not depend on the wing length, because there is no correlation among Figs. 6(b), (c), and (d).

The comparison among Figs. 6(a), (b), and (d) reveals the following. When the wing length is short, the shielding effect justly becomes low. When the wing length is long, the shielding effect tends to become high. However, the SPL does not decrease necessarily when the length is long. That is, it is the necessary condition to reduce the SPL at the side and bottom locations that the wing length is long. These knowledge in the design space corresponds to the exploration results, and the design information is discovered effectively and efficiently through the visualization on two-dimensional plane of SOM.

5 CONCLUSIONS

The multi-objective design exploration has been performed regarding the shielding effect of wing and fuselage to reduce the engine noise. In the present study, the two-dimensional problem is defined and the noise propagation is evaluated by using the linearized Euler equation at the side and bottom measuring locations relative to the fuselage. Moreover, a self-organizing map as a data mining technique is applied to this design exploration. As a result, there is no tradeoff between the objective functions, *i.e.*, the noise at two position of the side and bottom relative to the fuselage can be reduced simultaneously. It is essential key that the wing shields the sideward radiation of the sound pressure relative to the fuselage to reduce the sound pressure level at both of the side and bottom measuring location. Self-organizing maps obtain the design knowledge. When a wing spanwise length becomes larger, the shielding effect properly becomes strong. When the wing cant angle becomes 65deg to 68deg, which can be practically designed, the shielding effect is strongest. Data mining technique is an important facet of solving a multi-objective design exploration. In the present study, the mono-pole sound source as an engine noise and a lower frequency are assumed for the first step. The more practical design exploration will be defined.

REFERENCES

[1] A. Agarwal and A. P. Dowling, "The calculation of acoustic shielding of engine noise by the silent aircraft airframe," AIAA Paper 2005-2996, 2005.

[2] T. Imamura, K. Amemiya, S. Enomoto, and K. Yamamoto, "Development of linearized euler equation code and its application to complicated configuration," *Trans-*

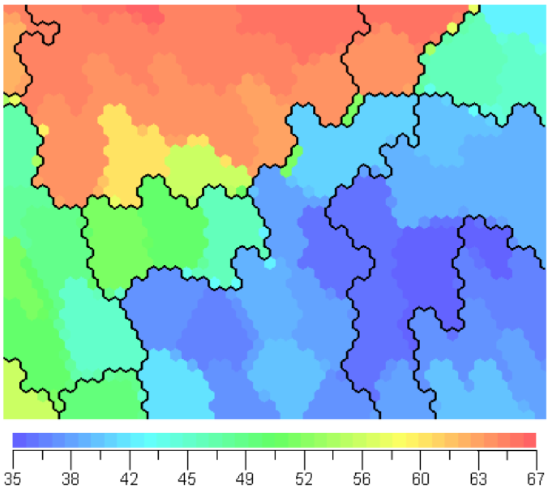

(a) Colored by the SPL at the side measuring location as the objective function 1

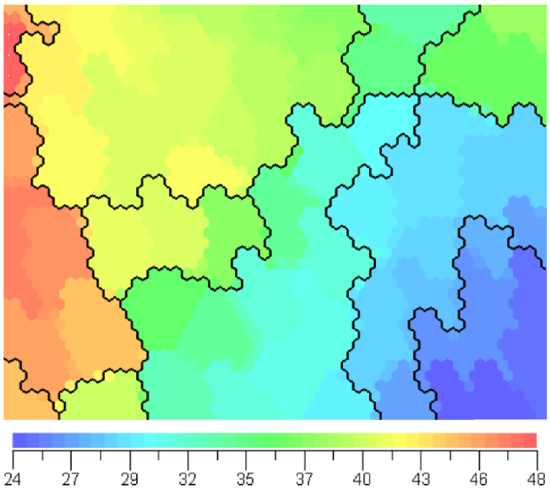

(b) Colored by the SPL at the bottom measuring location as the objective function 2

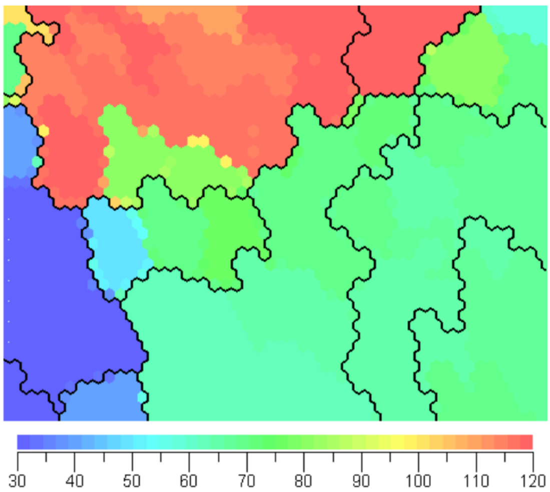

(c) Colored by the wing cant angle as the design variable 1

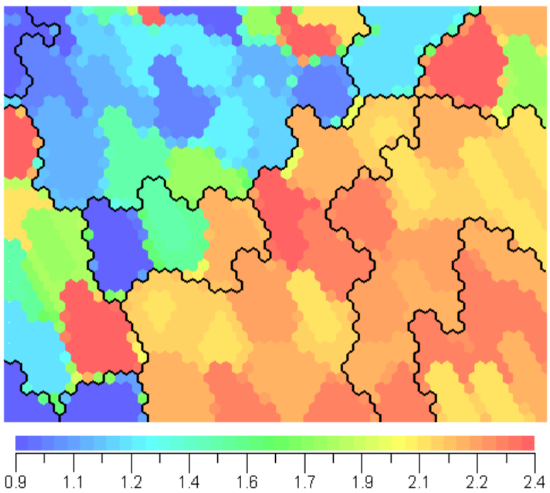

(d) Colored by the wing spanwise length as the design variable 2

Figure 6: SOM colored by the objective functions and the design variables.

actions of the Japan Society for Aeronautical and Space Sciences, vol. 53, no. 621, pp. 452–460, 2005.

[3] M. H. Kobayashi, "On a class of padé finite volume methods," *Journal of Computational Physics*, vol. 156, no. 1, pp. 137–180, 1999.

[4] D. V. Gaitonde and M. R. Visbal, "Padé-type higher order boundary filters for the navier-stokes equations," *AIAA Journal*, vol. 38, no. 11, pp. 2103–2112, 2000.

[5] A. Jameson and T. J. Baker, "Solution of the euler equations for complex configuration," AIAA Paper 83-1929, 1983.

[6] T. Colonius, S. K. Lele, and P. Moin, "Boundary conditions for direct computation of aerodynamic sound generation," *AIAA Journal*, vol. 31, no. 9, pp. 1574–1582, 1993.

[7] S. R. Chakravarthy and S. Osher, "Numerical experiments with the osher upwind scheme for the euler equations," *AIAA Journal*, vol. 21, no. 11, pp. 1241–1248, 1983.

[8] A. J. Keane, "Wing optimization using design of experiment, response surface, and data fusion methods," *Journal of Aircraft*, vol. 40, no. 4, pp. 741–750, 2003.

[9] S. Jeong, M. Murayama, and K. Yamamoto, "Efficient optimization design method using kriging model," *Journal of Aircraft*, vol. 42, no. 2, pp. 413–420, 2005.

[10] T. Kohonen, *Self-Organizing Maps.* Springer, Berlin, Heidelberg, 1995.

[11] "Eudaptics website," URL: http://www.eudaptics.com [cited 16 June 2004].

[12] G. Deboeck and T. Kohonen, *Visual Explorations in Finance with Self-Organizing Maps.* London, Springer Finance, 1998.

[13] E. Pampalk, A. Rauber, and D. Merkl, "Content-Based Organization and Visualization of Music Archives," in *Proceedings of the 10th International conference on Multimedie*, ACM Press, NY, 2002, pp. 570–579.

[14] J. Vesanto and E. Alhoniemi, "Clustering of the Self-Organizing Map," *IEEE Transactions on Neural Networks*, vol. 11, no. 3, pp. 586–600, 2000.

[15] S. Obayashi and D. Sasaki, "Visualization and data mining of pareto solutions using self-organizing map," in *EMO 2003, Lecture Notes in Computer Science 2632*, Springer-Verlag Heidelberg, Faro, Portugal, 2003, pp. 796–809.

[16] K. Chiba, S. Obayashi, K. Nakahashi, and H. Morino, "High-fidelity multidisciplinary design optimization of aerostructural wing shape for regional jet," AIAA Paper 2005-5080, 2005.